Nr. 21
04. September 2015

Leopold-Franzens-Universität Innsbruck

Preprint-Series: Department of Mathematics - Applied Mathematics

Sampeling Conditions for the circular Radon Transform

Markus Haltmeier

REVISED VERSION, APRIL 2016

Technikerstraße 13 - 6020 Innsbruck - Austria
Tel.: +43 512 507 53803 Fax: +43 512 507 53898
https://applied-math.uibk.ac.at

Sampling Conditions for the Circular Radon Transform

Markus Haltmeier

***Abstract*—Recovering a function from circular or spherical mean values is the basis of many modern imaging technologies, such as photo- and thermoacoustic computed tomography and ultrasound reflection tomography. Recently much progress has been made concerning the problem of recovering a function from its circular mean values. In particular, theoretically exact inversion formulas of the back-projection type have been discovered using continuously sampled data. In practical applications, however, only a discrete number of circular mean values can be collected. In this paper we address this issue in the context of Shannon sampling theory. We derive sharp sampling conditions for the number of angular and radial samples, respectively such that any essentially b_0-bandlimited function can be recovered from a finite number of such circular mean values.**

***Index Terms*—Spherical means, circular means, circular Radon transform, sampling theory, photoacoustic tomography, essentially bandlimited.**

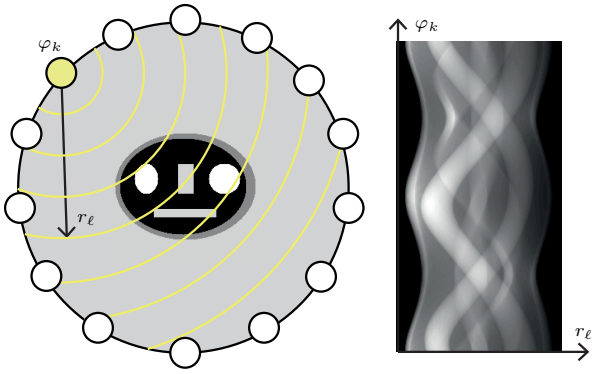

Fig. 1. INVERSION OF THE CIRCULAR RADON TRANSFORM. Left: Given are discrete number of averages $\mathbf{M}_R f(\varphi_k, r_\ell)$ over circles centered at $(R\cos\varphi_k, R\sin\varphi_k)$ and having radius r_ℓ. The aim is recovering the function f from the averages $\mathbf{M}_R f(\varphi_k, r_\ell)$ shown on the right hand side.

I. INTRODUCTION

MANY contemporary tomographic imaging applications require constructing a planar function $f\colon \mathbb{R}^2 \to \mathbb{R}$ from its *circular Radon transform*

$$\mathbf{M}_R f(\varphi, r) := \frac{1}{2\pi} \int_{\mathbb{S}^1} f(z(\varphi) + r\theta) \mathrm{d}\theta \,. \tag{1}$$

Here $\mathbb{S}^1 := \{\theta \in \mathbb{R}^2 \colon \|\theta\| = 1\}$ is the unit circle consisting of all elements in the plane with Euclidian norm $\|\cdot\|$ equal to one, $r \in \mathbb{R}$ is the radius and

$$z(\varphi) := \begin{bmatrix} R\cos(\varphi) \\ R\sin(\varphi) \end{bmatrix} \quad \text{for } \varphi \in \mathbb{R} \,, \tag{2}$$

the center of the circle of integration. According to our definition, $\mathbf{M}_R f$ is 2π-periodic in the first argument (the angular variable φ) and even in the second argument (the radial variable r). In tomographic applications, the function f represents a density function of some investigated object, and the circular Radon transform $\mathbf{M}_R f(\varphi, r)$ is the available indirect information; compare Figure 1. The index $R > 0$ is a prescribed parameter and indicates that the detectors are located on a circle of radius R surrounding the investigated object. In (1) and elsewhere the symbol $:=$ stands for *equal by definition*.

In this paper we study the problem of recovering f from the circular Radon transform $\mathbf{M}_R f$. In particular, we are interested in the practically relevant case, where only discrete samples of $\mathbf{M}_R f$ are available. We also study the closely related problem of reconstructing the initial data of the wave equation from discretely sampled boundary data. Among others, both reconstruction problems are relevant for photoacoustic and thermoacoustic tomography [1]–[4] or ultrasound reflection tomography [5], [6], [7, Chapter 8]. Photoacoustic tomography is based on three-dimensional wave propagation and therefore the two-dimensional model (1) may be seen a-physical. However, the two-dimensional problem actually arises in a variant that uses integrating line detectors for recording the pressure waves [2], [8]. In this so-called *tomography with integrating line detectors* an array of linearly shaped detectors is arranged around the investigated sample and records integrals of the pressure over a set of parallel lines. The integration along the direction of the line detectors reduces the dimensionality of the original three dimensional problem by one. Image reconstruction is performed via a two-stage approach, where in the first step projection images are obtained by inverting $\mathbf{M}_R f$. These projection images are already of valuable diagnostic use. Fully 3D image reconstruction is achieved by combining, in a second step, projection images from different views using the inverse classical Radon transform; see [2], [9], [10].

A. Inversion of the circular Radon transform

Especially, due to the relevance for thermo- and photoacoustic tomography, the circular Radon transform (as well as its analogon in three dimensional space, the spherical Radon transform) has been studied extensively in the recent years. In particular, several inversion methods have been derived using complete knowledge of the circular Radon transform. Suppose that f is supported in the disc $D(R) := \{x \in \mathbb{R}^2 : \|x\| < R\}$ of radius R centered at the origin. It is well known, that given the data $\mathbf{M}_R f(\varphi, r)$ for all $\varphi \in [0, 2\pi)$ and all $r > 0$, the unknown function f can be stably determined by means of

M. Haltmeier is with the Department of Mathematics, University of Innsbruck, Technikestraße 13, A-6020 Innsbruck, Austria.

explicit formulas of the filtered backprojection type (see, for example, [11]–[17]).

However, in practical applications only a discrete number of samples of $\mathbf{M}_R f$ can be collected, and numerical implementations of explicit inversion formulas (as any other reconstruction algorithm) deal with discrete data. Therefore, the question arises how many samples of the circular Radon transform should be collected for reliably representing the original function. For the classical Radon transform correct sampling is a well investigated issue (see, for example, [18]–[26]). For the circular Radon transform, however, sampling has hardly been addressed in the literature so far. We note that the classical and the circular Radon are indeed both special cases of the generalized Radon transform [27], which integrates a function over general families of curves (or surfaces) and can be used in many wave-equation based imaging applications. It is an interesting open issue to generalize sampling results from circular rays to more general curves, and to investigate the robustness of our sampling results to small deviations from exactly circular rays.

B. Discrete sampling

The standard sampling scheme for the circular Radon transform $\mathbf{M}_R f$ consists of uniformly sampled values

$$g(\varphi_k, r_\ell) := (\mathbf{M}_R f)(\varphi_k, r_\ell)\,, \tag{3}$$

where

$$\varphi_k := k\,\frac{2\pi}{N_\varphi} \qquad \text{for } k = 0, \dots, N_\varphi - 1\,, \tag{4}$$

$$r_\ell := R + \ell\,\frac{2R}{N_r} \qquad \text{for } \ell = -N_r/2, \dots, N_r/2\,, \tag{5}$$

are equidistant detector locations and radii, respectively. Here $N_\varphi \in \mathbb{N}$ is the number of angular samples and $N_r \in 2\mathbb{N}$ the number of radial samples within the interval $[0, 2R]$. Further, $2\pi/N_\varphi$ is the angular sampling step size and $2R/N_r$ the radial sampling step size.

Clearly, discrete data (3)-(5) are not sufficient for recovering an arbitrary function f. Instead, depending on the sampling step sizes, the function to be recovered must be restricted to a certain practically relevant function class. In this paper we address the sampling issue in the context of Shannon's sampling theory [28]–[31] using essentially bandlimited functions. Here the function f is called *essentially b_0-bandlimited* if its Fourier transform is sufficiently small outside the closed disc $\{\xi \in \mathbb{R}^2 \colon \|\xi\| \le b_0\}$. Note that for sampling the circular Radon transform we have to deal with functions that are compactly supported. Therefore, the Fourier transform of f cannot vanish exactly outside a bounded set; this is the reason we work with essentially bandlimited functions instead of strictly bandlimited ones.

C. Main results

Our main results concerning sampling the circular Radon transform can be summarized as follows:

1) Let $f \colon \mathbb{R}^2 \to \mathbb{R}$ be supported in $D(R)$ and be essentially b_0-bandlimited, in the sense that its Fourier transform is sufficiently small outside a disc of radius b_0. Then, provided that the sampling conditions

$$N_\varphi \ge 2Rb_0 \tag{6}$$

$$N_r \ge 2Rb_0/\pi \tag{7}$$

are satisfied, the discrete data (3)-(5) uniquely determine $\mathbf{M}_R f$ up to a small error, that depends on the frequency content of f outside $\{\xi \in \mathbb{R}^2 \colon \|\xi\| \le b_0\}$. As we show, such an approximation may be constructed by the two-dimensional Shannon sampling series. The obtained sampling conditions are sharp in the sense that no such estimate holds if N_φ and N_r do not satisfy (6), (7).

2) If, additionally, f is supported in a smaller disc $D(R_0)$, with $R_0 \le R$, then the number of angular samples can be reduced to $2R_0 b_0$. (Note that still, the data are collected on the circle with radius R.) Because in such a situation only $(R_0/R)N_r$ radial samples in (3) are different from zero, this shows, that a total number of M_0 circular mean values satisfying

$$M_0 \ge 4R_0^2 b_0^2/\pi$$

is sufficient to reliably represent any function f that is supported in $D(R_0)$ and has essential bandwidth b_0.

Both statements follow from results about the support of the two dimensional Fourier transform of $\mathbf{M}_R f$ that we derive in this paper (see Theorem IV.2), and the multi-dimensional sampling theorem for periodic functions reviewed in Section II. More precisely, Theorem IV.2 shows that the Fourier spectrum of $\mathbf{M}_R f$ is negligible outside a region that depends on R_0 and the Fourier spectrum of f. Using such information, the multi-dimensional sampling theorem of [29] provides sufficient conditions such that a discrete set of sampling points in $[0, 2\pi) \times \mathbb{R}$ stably determines $\mathbf{M}_R f$. Together with explicit inversion formulas of [9], [11]–[13] for recovering f from $\mathbf{M}_R f$ this implies that also f is stably determined by the discrete samples of $\mathbf{M}_R f$.

In many practical applications, such as photoacoustic tomography, radial (or temporal) samples can easily be collected at a high sampling rate compared to the spatial sampling, where each sample requires a separate sensor. Therefore a main practical implication of our results is giving a minimal number $N_\varphi = 2R_0 b_0$ of discrete detector locations required for sampling the circular Radon transform of an essentially b_0-bandlimited function supported in $D(R_0)$.

D. Notation

We denote by $C_c^\infty(D(R))$ the space of all C^∞-functions (that is, infinitely smooth functions) $f \colon \mathbb{R}^2 \to \mathbb{R}$ that have compact support in $D(R)$. Further, we denote by $C_{2\pi}^\infty(\mathbb{R}^2)$ the space of all C^∞-functions $g \colon \mathbb{R}^2 \to \mathbb{R}$ that are 2π-periodic in the first argument. For $f \in C_c^\infty(D(R))$ and $(z, r) \in \mathbb{R}^2 \times \mathbb{R}$ we define the circular mean values

$$\mathbf{M} f(z, r) := \frac{1}{2\pi} \int_{\mathbb{S}^1} f(z + r\theta)\mathrm{d}\theta$$

and write $\mathbf{M}_R f(\varphi, r) := \mathbf{M} f(z(\varphi), r)$, where $z(\varphi)$ is as in (2). Because the circular Radon transform $\mathbf{M}_R$ maps smooth

functions with support in $D(R)$ to functions in $C^\infty_{2\pi}(\mathbb{R}^2)$ we have $\mathbf{M}_R\colon C^\infty_c(D(R)) \to C^\infty_{2\pi}(\mathbb{R}^2)$. For the sake of simplicity, we assume throughout that the original function f is of class C^∞. As can been seen from the corresponding proofs, the main results in this paper (Theorem IV.2 and Theorem III.4) also hold for less smooth functions, whose Fourier transform shows sufficient decay at infinity.

We call a function $\eta\colon (0,1)\times(0,\infty)\to\mathbb{R}$ exponentially decreasing (in the second argument), if for every $c\in(0,1)$ there are constants $\lambda(c), d(c), Q(c) > 0$, such that $0 \le \eta(c,b) \le d(c)e^{-\lambda(c)b}$ for all $b\in\mathbb{R}$ with $b \ge Q(c)$. For $f\in C^\infty_c(D(R))$, $d\in\mathbb{R}$ and $b_0>0$ we define

$$\epsilon_d(f,b_0) := \int_{\|\xi\|>b_0} (\mathbf{F}f)(\xi)\|\xi\|^d \mathrm{d}\xi\,, \tag{8}$$

where $(\mathbf{F}f)(\xi) = (2\pi)^{-1}\int_{\mathbb{R}^2} e^{-i\langle\xi,x\rangle} f(x)\mathrm{d}x$ is the Fourier transform of f. If $\epsilon_1(f,b_0)$ is sufficiently small, we call f essentially b_0-bandlimited and name $\{\xi\in\mathbb{R}^2\colon \|\xi\|\le b_0\}$ the essential support of $\mathbf{F}f$. By requiring $\epsilon_1(f,b_0)$ to be bounded by a prescribed tolerance $\epsilon>0$ we could precise the notations of essential bandwidth and essential support. To avoid unnecessarily complicating our presentation we prefer to work with the qualitative notions of essential bandwidth and support.

For $g\in C^\infty_{2\pi}(\mathbb{R}^2)$ we write

$$(\mathbf{F}_t g)(\varphi,\omega) := \sqrt{\frac{1}{2\pi}}\int_{\mathbb{R}} g(\varphi,r)e^{-i\omega r}\mathrm{d}r \text{ with } (\varphi,\omega)\in\mathbb{R}^2$$

for the Fourier transform in the second component and

$$(\mathbf{F}g)(k,\omega) := \frac{1}{2\pi}\int_0^{2\pi}\int_{\mathbb{R}} g(\varphi,r)e^{-i(k\varphi+\omega r)}\mathrm{d}r\mathrm{d}\varphi$$

with $(k,\omega)\in\mathbb{Z}\times\mathbb{R}$ for the two-dimensional Fourier transform. The inverse two-dimensional Fourier transform is given by $(\mathbf{F}^{-1}\Phi)(\varphi,r) = 1/(2\pi)\int_{\mathbb{Z}\times\mathbb{R}}\Phi(k,\omega)e^{i(k\varphi+\omega r)}\mathrm{d}(k,\omega)$, where $\mathrm{d}(k,\omega)$ is the product of the counting measure on $\mathbb{Z}$ and the Lebesgue measure on $\mathbb{R}$. We call a compact subset $K\subseteq\mathbb{Z}\times\mathbb{R}$ essential support of $\Phi\colon\mathbb{Z}\times\mathbb{R}\to\mathbb{C}$ if the integral $\epsilon(\Phi,K) := \int_{(\mathbb{Z}\times\mathbb{R})\setminus K}|\Phi(k,\omega)|\mathrm{d}(k,\omega)$ is sufficiently small. Again this notion could be expressed in more quantitative terms by requiring $\epsilon(\Phi,K)$ to be smaller that a prescribed tolerance.

E. Outline

In Section II we review the multidimensional sampling theorem on $C^\infty_{2\pi}(\mathbb{R}^2)$. In Section III we consider sampling of solutions of the wave equation. Besides investigating the standard sampling scheme, for the wave data we derive a more efficient sampling scheme in the form of the interlaced lattice. The obtained results for the wave equation will be used to derive sampling conditions for the circular Radon transform in Section IV. The paper concludes with a short discussion presented in Section V.

II. Sampling on $[0,2\pi)\times\mathbb{R}$

The multi-dimensional sampling theorem of [29] considers Shannon sampling theory on non-orthogonal grids. In this section we present a variant of the multi-dimensional sampling theorem (taken from [21], [25]) for sampling periodic functions. This theorem is non-standard because it allows both, non-Cartesian sampling and periodic functions.

Definition II.1 (Admissible sampling lattice)**.** Let $W\in\mathbb{R}^{2\times2}$ be any invertible matrix. Then $L_W := W\mathbb{Z}^2\cap([0,2\pi)\times\mathbb{R})$ is called admissible sampling lattice for $[0,2\pi)\times\mathbb{R}$ generated by W, if $(2\pi,0)\in W\mathbb{Z}^2$ and $(0,r)\in L_W$ for some $r>0$.

In Definition II.1, $W\mathbb{Z}^2 = \{Wm : m\in\mathbb{Z}^2\}$ denotes the set of all integer linear combinations of columns of W. Note that an admissible sampling lattice L_W may be generated by different matrices. However, one can show that $|\det W|$ and $2\pi W^{-\mathsf{T}}\mathbb{Z}^2$ (the so called dual lattice) are uniquely determined by L_W. Here and in the following we use the notation $W^{-\mathsf{T}} := (W^{\mathsf{T}})^{-1}$

Theorem II.2 (Sampling theorem on $[0,2\pi)\times\mathbb{R}$)**.** *Let L_W be an admissible sampling lattice for $[0,2\pi)\times\mathbb{R}$, and let $K\subseteq\mathbb{Z}\times\mathbb{R}$ be a compact set such that the sampling condition*

$$\forall m\in\mathbb{Z}^2\colon\quad K^\circ\cap\left(K^\circ + 2\pi W^{-\mathsf{T}}m\right) = \emptyset \tag{9}$$

holds, where K° denotes the interior of K. Suppose $g\in C^\infty_{2\pi}(\mathbb{R}^2)$, denote by χ_K the characteristic function of K, and define the sampling series

$$(\mathbf{S}_{W,K}g)(\varphi,r) := \frac{|\det(W)|}{2\pi}\sum_{v\in L_W}\left(\mathbf{F}^{-1}\chi_K\right)((\varphi,r)-v)g(v)\,.$$

Then, $\|\mathbf{S}_{W,K}g - g\|_\infty \le \pi^{-1}\int_{\mathbb{R}^n\setminus K}|\mathbf{F}g(k,\omega)|\mathrm{d}(k,\omega)$.

Proof: See [21], [25]. ∎

Theorem II.2 states that the discrete samples $(g(v))_{v\in L_W}$ uniquely determine an approximation to g (namely the sampling series $\mathbf{S}_{W,K}g$), provided that (9) is satisfied and that the Fourier transform $\mathbf{F}g$ is small outside K.

Important admissible sampling lattices are the standard lattice $\{(2\pi k/N_\varphi, h_s\ell)\colon k\in\{0,\dots,N_\varphi-1\},\ell\in\mathbb{Z}\}$ and the interlaced lattice $\{(2\pi k/N_\varphi, 2h_s(\ell+k/2))\colon k\in\{0,\dots,N_\varphi-1\},\ell\in\mathbb{Z}\}$. For the standard lattice, W is a diagonal matrix with diagonal entries $2\pi/N_\varphi$ and h_s. For the interlaced lattice, W is a lower triangular matrix, whose first column equals $[2\pi/N_\varphi, h_s]^{\mathsf{T}}$ and whose second column equals $[0, 2h_s]^{\mathsf{T}}$. Among others, these lattices are relevant for sampling the standard Radon transform, where the interlaced lattice yields the same resolution as the standard lattice using only half the number of sampling points [21], [25], [26]. In this paper we derive a similar result for sampling the wave equation. For the circular Radon transform, the theory developed in this paper only supports the standard lattice.

III. Sampling the wave equation

Inverting the circular Radon transform is closely related to the problem of reconstructing the initial data of the wave

equation from its solution observed at certain detector locations. Actually, in applications like photoacoustic tomography, the measurement data are given by the solution of the wave equation. In this section we derive sampling conditions for the solution of the wave equation on a circle using either the standard or the interlaced lattice. We will show that the interlaced lattice yields the same resolution as the standard lattice using only half the number of sampling points.

A. The wave equation

For $f \in C_c^\infty(D(R))$ consider the wave equation

$$(\partial_t^2 - \Delta_x)\, u(x,t) = 0 \qquad \text{for } (x,t) \in \mathbb{R}^2 \times (0,\infty) \tag{10}$$

$$u(x,0) = f(x) \qquad \text{for } x \in \mathbb{R}^2 \tag{11}$$

$$(\partial_t u)(x,0) = 0 \qquad \text{for } x \in \mathbb{R}^2\,. \tag{12}$$

We denote by $\mathbf{U}f\colon \mathbb{R}^2 \times \mathbb{R} \to \mathbb{R}$ the solution of (10)-(12) extended to an even function in t. The fact that (10)-(12) has a unique solution [32, Chap. 2.4] implies that $\mathbf{U}f$ is a well-defined function. The restriction of $\mathbf{U}f$ to the boundary of $D(R)$ is denoted by $\mathbf{U}_R f(\varphi,t) := \mathbf{U}f(z(\varphi),t)$ for $(\varphi,t) \in \mathbb{R}^2$. Our aim is to recover f from discrete samples of $\mathbf{U}_R f$.

The solution of the wave equation (10)-(12) can be expressed in terms of the circular Radon transform by

$$(\mathbf{U}f)(z,t) = \partial_t \mathbf{A}_t \mathbf{M}(z,t) = \frac{\partial}{\partial t}\int_0^t \frac{r\mathbf{M}f(z,r)}{\sqrt{t^2-r^2}}\,\mathrm{d}r\,, \tag{13}$$

where $(\mathbf{A}_t g)(z,t) := \int_0^t (t^2-r^2)^{-1/2} g(z,r) r \mathrm{d}r$ is the Abel transform with respect to the second variable [11, Eq. (11)]. The known inversion formula of the Abel transform implies that we can also express the circular Radon transform in terms of the wave equation $\mathbf{M}_R f = (2/\pi)\mathbf{A}_t t^{-1} \mathbf{U}_R f$; see [9].

B. Auxiliary results

In the following we frequently make use of the Bessel function $J_\nu\colon \mathbb{R} \to \mathbb{R}$ order $\nu \in \mathbb{R}$, defined by

$$J_\nu(x) := \left(\frac{x}{2}\right)^\nu \sum_{k=0}^\infty \frac{(-x^2/4)^k}{k!\,\Gamma(k+\nu+1)} \qquad \text{for } x \in \mathbb{R}\,,$$

with $\Gamma(z) := \int_0^\infty t^{z-1}e^{-t}\mathrm{d}t$ denoting the Gamma function.

We first derive some useful expressions for $\mathbf{F}\mathbf{U}_R f$.

Lemma III.1. *For $f \in C_c^\infty(D(R))$ and $(k,\omega) \in \mathbb{Z} \times \mathbb{R}$,*

$$(\mathbf{F}\mathbf{U}_R f)(k,\omega) = \frac{i^k}{2}|\omega| J_k(\omega R) \int_{\mathbb{S}^1} (\mathbf{F}f)(\omega\theta) e^{-ik\alpha}\mathrm{d}\alpha \tag{14}$$

$$= \frac{|\omega|}{2} J_k(\omega R) \int_{\mathbb{R}^2} f(x) e^{-ik\beta\|x\|} J_k(\omega\|x\|)\mathrm{d}x\,, \tag{15}$$

with $\theta = (\cos(\alpha),\sin(\alpha))$ and $x = \|x\|(\cos(\beta),\sin(\beta))$.

Proof: See Appendix A. ∎

For the following results recall the notion of an exponentially decreasing function $\eta(c,b)$, and the approximation error $\epsilon_d(f,b)$ introduced in Section I-D.

Lemma III.2.

1) *The following functions $\eta_i\colon (0,1)\times[0,\infty) \to \mathbb{R}$ are exponentially decreasing:*
   - $\eta_1(c,b) := J_b(cb)$;
   - $\eta_2(c,b) := \sup_{r\in[0,R_0]} \int_{-cb/R_0}^{cb/R_0} |J_b(r\omega)|\mathrm{d}\omega$;
   - $\eta_3(c,b) := \sum_{m\geq b} \eta_2(c,m)$.
2) $\sum_{k\in\mathbb{N}, k\geq b/c} \epsilon_d(f,ck) \leq (1/c)\,\epsilon_{d+1}(f,b)$.

Proof: See [25, p. 66]. ∎

The following estimates are main ingredients for finding the essential support of $\mathbf{F}\mathbf{U}_R f$.

Lemma III.3. *For $f \in C_c^\infty(D(R))$ and $(k,b_0) \in \mathbb{Z}\times\mathbb{R}$,*

1) $\int_{|\omega|>b_0} |(\mathbf{F}\mathbf{U}_R f)(k,\omega)|\mathrm{d}\omega \leq \epsilon_0(f,b_0)$;
2) $\int_{|\omega|<\frac{c}{R_0}|k|} |(\mathbf{F}\mathbf{U}_R f)(k,\omega)|\mathrm{d}\omega \leq \frac{1}{2}\eta_2(c,|k|)\,\|f\|_{L^1}$.

Proof: 1) By (14) we have

$$|(\mathbf{F}\mathbf{U}_R f)(k,\omega)| \leq \frac{|\omega|}{2}|J_k(\omega R)| \left|\int_{\mathbb{S}^1} (\mathbf{F}f)(\omega\theta) e^{-ik\varphi}\mathrm{d}\theta\right| \leq \frac{|\omega|}{2}\int_{\mathbb{S}^1} |\mathbf{F}f(\omega\theta)|\mathrm{d}\theta\,,$$

where the last equality follows from $|J_k(\omega R)| \leq 1$. Consequently, by introducing polar coordinates $\xi = \omega\theta$

$$\int_{|\omega|>b_0} |(\mathbf{F}\mathbf{U}_R f)(k,\omega)|\mathrm{d}\omega \leq \frac{1}{2}\int_{|\omega|>b_0}\int_{\mathbb{S}^1} |\omega||\mathbf{F}f(\omega\theta)|\mathrm{d}\theta\mathrm{d}\omega = \int_{\|\xi\|>b_0} |\mathbf{F}f(\xi)|\mathrm{d}\xi = \epsilon_0(f)\,.$$

2) By (15) we have

$$\begin{aligned}
&\int_{|\omega|<\frac{c}{R_0}|k|} |(\mathbf{F}\mathbf{U}_R f)(k,\omega)|\mathrm{d}\omega \\
&\leq \int_{|\omega|<\frac{c}{R_0}|k|} \frac{|\omega||J_k(\omega R)|}{2} \int_{D(R_0)} |f(x)|\,|J_k(\omega\|x\|)|\mathrm{d}x\mathrm{d}\omega \\
&\leq \frac{1}{2}\int_{D(R_0)} |f(x)| \int_{|\omega|<\frac{c}{R_0}|k|} |\omega|\,|J_k(\omega\|x\|)|\mathrm{d}\omega\mathrm{d}x \\
&\leq \frac{1}{2}\|f\|_{L^1} \sup_{r\in[0,R_0]} \int_{|\omega|<\frac{c}{R_0}|k|} |\omega|\,|J_k(\omega r)|\mathrm{d}\omega\,.
\end{aligned}$$

Inserting the definition of η_2 concludes the proof. ∎

C. Essential support of $\mathbf{F}\mathbf{U}_R f$

For $b_0 > 0$, $R_0 \in (0,R]$ and $c \in (0,1)$ define

$$S(c,b_0,R_0) := \Big\{(k,\omega) \in \mathbb{Z}\times\mathbb{R}\colon |\omega| < b_0 \text{ and } |k| \leq \frac{R_0}{c}\max\{|\omega|,(1-c)b_0\}\Big\}\,, \tag{16}$$

see Figure 2. The following theorem states that $S(c,b_0,R_0)$ contains the essential support of $\mathbf{F}\mathbf{U}_R f$ provided that $f \in C_c^\infty(D(R_0))$ is essentially b_0-bandlimited.

Theorem III.4 (Essential support of $\mathbf{F}\mathbf{U}_R f$)**.** *There exists an exponentially decreasing $\eta\colon (0,1)\times(0,\infty) \to \mathbb{R}$, such that for $b_0 > 0$, $R_0 \in (0,R]$, $c \in (0,1)$ and $f \in C_c^\infty(D(R_0))$,*

$$\int_{(\mathbb{Z}\times\mathbb{R})\setminus S(c,b_0,R_0)} |(\mathbf{F}\mathbf{U}_R f)(k,\omega)|\,\mathrm{d}(k,\omega) \leq \frac{4}{c}\,\epsilon_1(f,b_0) + \eta\,(c,b_0)\,\|f\|_{L^1}\,. \quad (17)$$

Proof: We write $(\mathbb{Z}\times\mathbb{R})\setminus S(c,b_0,R_0) = M_1\cup M_2\cup M_3$, where

- $M_1 \coloneqq \{(k,\omega)\colon |\omega| < c|k|/R_0 \text{ and } |k| > R_0 b_0(1/c-1)\}$;
- $M_2 \coloneqq \{(k,\omega)\colon |\omega| \geq b_0 \text{ and } |k| < R_0 b_0/c\}$;
- $M_3 \coloneqq \{(k,\omega)\colon |\omega| > c|k|/R_0 \text{ and } |k| \geq R_0 b_0/c\}$.

We proceed by estimating the integral of $|(\mathbf{F}\mathbf{U}_R f)(k,\omega)|$ over any of the domains M_i. For that purpose we frequently use Lemmas III.2 and III.3:

- First, the integral over M_1 satisfies

$$\begin{aligned} I_1 &\coloneqq \int_{M_1} |(\mathbf{F}\mathbf{U}_R f)(k,\omega)|\,\mathrm{d}(k,\omega) \\ &= \sum_{k>R_0b_0(1/c-1)} \int_{|\omega|<c\frac{|k|}{R_0}} |\mathbf{F}\mathbf{U}_R f(k,\omega)|\,\mathrm{d}\omega \\ &\leq \|f\|_{L^1} \sum_{k>R_0b_0(1/c-1)} \eta_2\,(c,|k|) \\ &= \|f\|_{L^1}\, 2\eta_3(c, R_0b_0(1/c-1))\,. \end{aligned}$$

  In the above, the first inequality follows from statement 2) in Lemma III.3 and last equality uses the definition of the exponentially decreasing function η_3 given in statement 1) in Lemma III.2.
- Next, the integral over M_2 is estimated as

$$\begin{aligned} I_2 &\coloneqq \int_{M_2} |(\mathbf{F}\mathbf{U}_R f)(k,\omega)|\,\mathrm{d}(k,\omega) \\ &= \sum_{k<Rb_0/c} \int_{|\omega|\geq b_0} |\mathbf{F}\mathbf{U}_R f(k,\omega)|\,\mathrm{d}\omega \\ &\leq (2R_0b_0/c)\,\epsilon_0(f,b_0) \\ &\leq (2R_0/c)\,\epsilon_1(f,b_0)\,. \end{aligned}$$

  In the above, the first inequality follows from statement 1) in Lemma III.3.
- Finally, the integral over M_3 is estimated as

$$\begin{aligned} I_3 &\coloneqq \int_{M_3} |(\mathbf{F}\mathbf{U}_R f)(k,\omega)|\,\mathrm{d}(k,\omega) \\ &= \sum_{k\geq R_0b_0/c} \int_{|\omega|>c|k|/R_0} |\mathbf{F}\mathbf{U}_R f(k,\omega)|\,\mathrm{d}\omega \\ &\leq 2\sum_{k\geq Rb_0/c} \epsilon_0\,(f, c|k|/R_0) \\ &\leq (2R_0/c)\epsilon_1(f,b_0)\,. \end{aligned}$$

Combing these estimates yields

$$\begin{aligned} \int_{(\mathbb{Z}\times\mathbb{R})\setminus(c,b_0,R_0)} |\mathbf{F}\mathbf{U}_R f(k,\omega)|\,\mathrm{d}(k,\omega) &= I_1+I_2+I_3 \\ &\leq \frac{4R_0}{c}\epsilon_1(f,b_0) + 2\eta_3(c,R_0b_0(1/c-1))\,\|f\|_{L^1}\,. \end{aligned}$$

Setting $\eta(c,b_0) = 2\eta_3(c,R_0b_0(1/c-1))$ shows the claim and concludes the proof. ∎

D. Sampling schemes for $\mathbf{U}_R f$

Let $b_0 > 0$, $R_0 \in (0,R]$ and suppose that $f \in C_c^\infty(D(R_0))$ is essentially b_0-bandlimited in the sense that $\epsilon_1(f,b_0)$ is sufficiently small. For example, we may assume $\epsilon_1(f,b_0)$ being smaller than the measurement accuracy of the ultrasound detection system. Further let $L_W = W\mathbb{Z}^2 \cap [0,2\pi)\times\mathbb{R}$ be an admissible sampling lattice generated by $W \in \mathbb{R}^{2\times 2}$.

According to Theorems II.2 and III.4 the discrete values $(\mathbf{U}_R f(v))_{v\in L_W}$ stably represent $\mathbf{U}_R f$ if, for all $m \in \mathbb{Z}^2$,

$$S(c,b_0,R_0)^\circ \cap \big(S(c,b_0,R_0)^\circ + 2\pi W^{-\mathsf{T}} m\big) = \emptyset\,, \quad (18)$$

where $c \in (0,1)$ and $S(c,b_0,R_0)$ is defined by (16). Hence, one has to choose $2\pi W^{-\mathsf{T}}$ such that the translates $S(c,b_0,R_0)^\circ + 2\pi W^{-\mathsf{T}} m$ are disjoint to each other. In the following we will construct two appropriate sampling schemes: The standard (rectangular) sampling scheme and the interlaced sampling scheme.

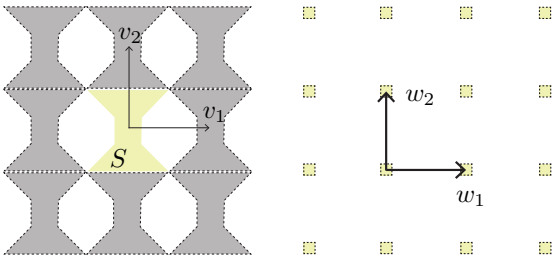

Fig. 2. STANDARD SAMPLING SCHEME FOR $\mathbf{U}_R f$. Left: The set $S = S(c,b_0,R_0)$ is translated along a rectangular grid such that $S \cap (S + 2\pi W^{-\mathsf{T}} m) = \emptyset$ (v_1 and v_2 denote the columns of $2\pi W^{-\mathsf{T}}$). Right: Resulting standard lattice (w_1 and w_2 denote the columns of W).

1) Standard Sampling scheme: For the standard sampling scheme one takes W as a diagonal matrix. From Figure 2 we see that the choice

$$2\pi W^{-\mathsf{T}} = \begin{bmatrix} 2R_0b_0/c & 0 \\ 0 & 2b_0 \end{bmatrix}$$

satisfies (18). Consequently,

$$W = \begin{bmatrix} c\pi/(R_0b_0) & 0 \\ 0 & \pi/b_0 \end{bmatrix} =: \begin{bmatrix} 2\pi/N_\varphi & 0 \\ 0 & 2R/N_t \end{bmatrix}$$

defines an admissible lattice. (We implicitly assume that N_φ and $N_t/2$ are integer numbers; otherwise we replace them by $\lceil N_\varphi\rceil$ and $\lceil N_t/2\rceil$.)

This yields the standard sampling scheme

$$\begin{aligned} g_{k,\ell} &\coloneqq (\mathbf{U}_R f)(\varphi_k, t_\ell) && (19)\\ \varphi_k &\coloneqq k2\pi/N_\varphi\,, && \text{for } 0\leq k\leq N_\varphi-1 \quad (20)\\ t_\ell &\coloneqq R+\ell 2R_0/N_t\,, && \text{for } |\ell|\leq N_t/2\,. \quad (21) \end{aligned}$$

Here, N_φ is the number of angular samples and N_t the number of temporal samples in the interval $[R-R_0, R+R_0]$. Taking $c\to 1$, we obtain the sampling conditions

$$\begin{aligned} N_\varphi &\geq 2R_0b_0 \\ N_t &\geq 2R_0b_0/\pi\,. \end{aligned}$$

They are the same as for the circular Radon transform (compare (6), (7) for the special case $R_0 = R$). Recall that

$\eta_1(c,b) = J_b(cb)$ is exponentially decreasing for any $c < 1$. Taking $c \to 1$ means we consider the largest parameter, where we have necessary decay of η_1.

Note that the condition $N_\varphi \geq 2R_0b_0$ has been derived in a different manner in [33, Section III-B].

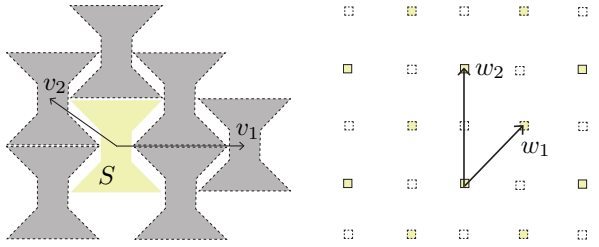

Fig. 3. INTERLACED SAMPLING SCHEME FOR $\mathbf{U}_R f$. Left: The set $S = S(c, b_0, R_0)$ is translated along non-orthogonal vectors such that the sets $2\pi W^{-\mathsf{T}} m + S$ are disjoint. Right: Resulting interlaced sampling scheme.

2) Interlaced sampling scheme: The standard lattice uses orthogonal translates of $S(c, b_0, R_0)$ which yield a non-optimal covering of the frequency domain. As illustrated in Figure 3, a denser covering is obtained by the choice

$$2\pi W^{-\mathsf{T}} = \begin{bmatrix} 2R_0b_0(2/c-1) & -R_0b_0(2/c-1) \\ 0 & b_0 \end{bmatrix},$$

which gives

$$W = \begin{bmatrix} (c\pi)/(R_0b_0(2-c)) & 0 \\ \pi/b_0 & 2\pi/b_0 \end{bmatrix} =: \begin{bmatrix} 2\pi/N_\varphi & 0 \\ R_0/N_t & 2R_0/N_t \end{bmatrix}.$$

Again, $2\pi/N_\varphi$ is angular sampling step size and $2R_0/N_t$ the temporal sampling step size.

Taking the limit $c \to 1$ we obtain the interlaced sampling scheme

$$g_{k,\ell} := (\mathbf{U}_R f)(\varphi_k, t_{k,\ell}) \tag{22}$$
$$\varphi_k := k2\pi/N_\varphi\,, \qquad 0 \leq k \leq N_\varphi - 1 \tag{23}$$
$$t_{k,\ell} := R + \ell\, 2R_0/N_t + kR_0/N_t\,, \quad |\ell| \leq N_t/2 \tag{24}$$

and the sampling conditions

$$N_\varphi \geq 2R_0b_0$$
$$N_t \geq R_0b_0/\pi\,.$$

The interlaced sampling scheme (22)-(24) requires only half of the sampling points of the standard lattice (19)-(21).

IV. SAMPLING THE CIRCULAR RADON TRANSFORM

In this section we investigate sampling the circular Radon transform. For that purpose we will exploit relations between the circular Radon transform and the wave equation.

A. Auxiliary result

We first derive a relation between $\mathbf{F}\mathbf{M}_R f$ and $\mathbf{F}\mathbf{U}_R f$.

Lemma IV.1. *For $f \in C_c^\infty(D(R))$ and $(k,\rho) \in \mathbb{Z}\times\mathbb{R}$,*

$$(\mathbf{F}\mathbf{M}_R f)(k,\rho) = \frac{2}{\pi}\int_\rho^\infty \frac{(\mathbf{F}\mathbf{U}_R f)(k,\omega)}{\sqrt{\omega^2-\rho^2}}\mathrm{d}\omega\,.$$

Proof: By (13) and using integration by parts,

$$\begin{aligned}
&(\mathbf{F}_t\mathbf{U}_R f)(\varphi,\omega) \\
&= \sqrt{\frac{2}{\pi}}\int_0^\infty \cos(\omega t)\frac{\partial}{\partial t}\int_0^t \frac{r\mathbf{M}_R f(\varphi,r)}{\sqrt{t^2-r^2}}\,\mathrm{d}r\,\mathrm{d}t \\
&= \sqrt{\frac{2}{\pi}}\omega\int_0^\infty \sin(\omega t)\int_0^t \frac{r\mathbf{M}_R f(\varphi,r)}{\sqrt{t^2-r^2}}\,\mathrm{d}r\,\mathrm{d}t \\
&= \sqrt{\frac{2}{\pi}}\omega\int_0^\infty r\mathbf{M}_R f(\varphi,r)\left(\int_r^\infty \frac{\sin(\omega t)}{\sqrt{t^2-r^2}}\,\mathrm{d}t\right)\mathrm{d}r\,.
\end{aligned}$$

The inner integral in the last equation is given by $\frac{\pi}{2}J_0(r\omega)$ (see, for example, [34, page 69, formula (8)]. Consequently,

$$(\mathbf{F}_t\mathbf{U}_R f)(\varphi,\omega) = \sqrt{\frac{\pi}{2}}\omega\mathbf{H}_t\mathbf{M}_R f(\varphi,\omega)\,, \tag{25}$$

where $(\mathbf{H}_t g)(z,\omega) := \int_0^\infty g(z,r)J_0(\omega r)r\mathrm{d}r$ denotes the zero-order Hankel transform in the second component.

Next recall $J_0(y) = \frac{1}{\pi}\int_{-1}^1 e^{izy}(1-z^2)^{-1/2}\mathrm{d}z$. Together with (25) and the Hankel inversion formula this yields

$$\begin{aligned}
&\mathbf{M}_R f(\varphi,r) \\
&= \frac{2}{\pi}\int_0^\infty J_0(\omega r)(\mathbf{F}_t\mathbf{M}_R f)(\varphi,\omega)\mathrm{d}\omega \\
&= \left(\frac{2}{\pi}\right)^{3/2}\int_0^\infty\int_0^\omega \cos(\rho r)\frac{\mathrm{d}\rho}{\sqrt{\omega^2-\rho^2}}(\mathbf{F}_t\mathbf{U}_R f)(\varphi,\omega)\mathrm{d}\omega \\
&= \left(\frac{2}{\pi}\right)^{3/2}\int_0^\infty \cos(\rho r)\int_\rho^\infty \frac{(\mathbf{F}_t\mathbf{U}_R f)(\varphi,\omega)}{\sqrt{\omega^2-\rho^2}}\mathrm{d}\omega\mathrm{d}\rho\,.
\end{aligned}$$

Application of the two dimensional Fourier transform yields the desired result. ∎

B. Essential support of $\mathbf{F}\mathbf{M}_R f$

Now we are ready to formulate our main result which answers how to sample the circular Radon transform.

For $b_0, R_0 > 0$, $c \in (0,1)$ define

$$\begin{aligned}
Q(b_0R_0/c, b_0) &:= \left[-\frac{R_0b_0}{c}, \frac{R_0b_0}{c}\right]\times[-b_0,b_0] \\
&:= \left\{(k,\omega)\in\mathbb{Z}\times\mathbb{R}\colon |k| \leq \frac{R_0b_0}{c} \text{ and } |\omega| < b_0\right\}.
\end{aligned} \tag{26}$$

The following theorem states that $Q(b_0R_0/c, b_0)$ contains the essential support of $\mathbf{F}\mathbf{M}_R f$ provided that f is essentially b_0-bandlimited and supported in $D(R_0)$. As can be seen in Figure 4, the sets $Q(b_0R_0/c, b_0)$ have rectangular shape depending on two parameters. On the other hand, the sets $S(c, b_0, R_0)$ look similar to a sandglass and depend on an additional third parameter (see Figure 2).

Theorem IV.2 (Essential support of $\mathbf{F}\mathbf{M}_R f$)**.** *There exists an exponentially decreasing function $\eta\colon (0,1)\times(0,\infty)\to\mathbb{R}$ such that for every $b_0 > 0$, $R_0 \in (0,R]$ and $c \in (0,1)$ and every $f \in C_c^\infty(D(R_0))$, we have*

$$\begin{aligned}
&\int_{(\mathbb{Z}\times\mathbb{R})\setminus Q(b_0R_0/c,b_0)} |(\mathbf{F}\mathbf{M}_R f)(k,\rho)|\,\mathrm{d}(k,\rho) \\
&\qquad \leq \frac{4}{c}\,\epsilon_1(f,b_0) + \eta(c,b_0)\,\|f\|_{L^1}\,.
\end{aligned} \tag{27}$$

Proof: By Lemma IV.1 for every $a > 0$, we have

$$\begin{aligned}
&\int_a^\infty |(\mathbf{FM}_R f)(k,\rho)|\,\mathrm{d}\rho \\
&\quad\le \frac{2}{\pi}\int_a^\infty |(\mathbf{FU}_R f)(k,\omega)| \int_a^\rho \frac{\mathrm{d}\rho}{\sqrt{\omega^2-\rho^2}}\mathrm{d}\omega \\
&\quad\le \frac{2}{\pi}\int_a^\infty |(\mathbf{FU}_R f)(k,\omega)| \int_0^\rho \frac{\mathrm{d}\rho}{\sqrt{\omega^2-\rho^2}}\mathrm{d}\omega \\
&\quad\le \int_a^\infty |(\mathbf{FU}_R f)(k,\omega)|\,\mathrm{d}\omega\,.
\end{aligned}$$

This implies

$$\begin{aligned}
&\int_{(\mathbb{Z}\times\mathbb{R})\setminus Q(b_0R_0/c,b_0)} |(\mathbf{FM}_R f)(k,\rho)|\,\mathrm{d}(k,\rho) \\
&= 2\sum_{|k|\le Rb_0/c}\int_{b_0}^\infty |(\mathbf{FM}_R f)(k,\rho)|\,\mathrm{d}\rho \\
&\quad + 2\sum_{|k|>b_0R_0/c}\int_0^\infty |(\mathbf{FM}_R f)(k,\rho)|\,\mathrm{d}\rho \\
&\le 2\sum_{|k|\le b_0R_0/c}\int_{b_0}^\infty |(\mathbf{FU}_R f)(k,\rho)|\,\mathrm{d}\rho \\
&\quad + 2\sum_{|k|>b_0R_0/c}\int_0^\infty |(\mathbf{FU}_R f)(k,\rho)|\,\mathrm{d}\rho \\
&= \int_{(\mathbb{Z}\times\mathbb{R})\setminus Q(b_0R_0/c,b_0)} |(\mathbf{FU}_R f)(k,\omega)|\,\mathrm{d}(k,\omega)\,.
\end{aligned}$$

Now we have $(\mathbb{Z}\times\mathbb{R})\setminus Q(b_0R_0/c,b_0) \subseteq (\mathbb{Z}\times\mathbb{R})\setminus S(c,b_0,R_0)$, where $S(c,b_0,R_0)$ is defined by (17). Consequently, (27) follows from Theorem III.4. ∎

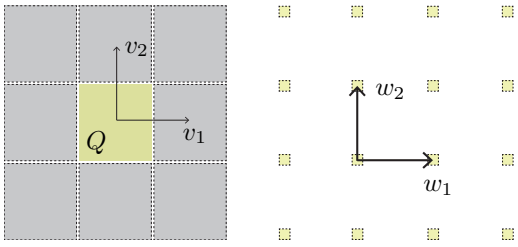

Fig. 4. STANDARD SAMPLING SCHEME FOR $\mathbf{M}_R f$. Left: The set $Q = Q(b_0R_0/c, b_0)$ and disjoint translates $Q(b_0R_0/c, b_0) + 2\pi W^{-\mathsf{T}} m$. Right: Resulting standard sampling scheme.

C. Standard sampling scheme for $\mathbf{M}_R f$

Suppose that $f \in C_c^\infty(D(R_0))$ with $R_0 \le R$ is essentially b_0-bandlimited, and let L_W be an admissible sampling lattice corresponding to $W \in \mathbb{R}^{2\times 2}$. According to Theorems II.2 and III.4 the discrete values $(\mathbf{M}_R f(v))_{v\in L_W}$ stably represent $\mathbf{M}_R f$ if for $m \in \mathbb{Z}^2$,

$$Q(b_0R_0/c,b_0)^\circ \cap \left(Q(b_0R_0/c,b_0)^\circ + 2\pi W^{-\mathsf{T}} m\right) = \emptyset\,,$$

where $c \in (0,1)$ and $Q(b_0R_0/c,b_0)$ is defined by (16).

Because $Q(b_0R_0/c,b_0)$ has rectangular shape (see Figure 4), an optimal covering of the $\mathbb{R}^2$ with disjoint translates $Q(b_0R_0/c,b_0) + 2\pi W^{-\mathsf{T}} m$ is obtained by

$$W = \begin{bmatrix} c\pi/(R_0b_0) & 0 \\ 0 & \pi/b_0 \end{bmatrix} =: \begin{bmatrix} 2\pi/N_\varphi & 0 \\ 0 & 2R_0/N_r \end{bmatrix}.$$

Here $2\pi/N_\varphi$ is the angular step size and $2a/N_r$ the radial step size. N_φ is the number of angular samples and N_r the number of radial samples in the interval $[R-R_0, R+R_0]$.

Taking $c \to 1$, yields the standard sampling scheme

$$\begin{aligned}
g_{k,\ell} &:= (\mathbf{M}_R f)(\varphi_k, r_\ell) \\
\varphi_k &:= k2\pi/N_\varphi\,, && \text{for } 0 \le k \le N_\varphi - 1 \\
r_\ell &:= R/2 + \ell\, 2R_0/N_r\,, && \text{for } |\ell| \le N_r/2
\end{aligned}$$

with the sampling conditions

$$\begin{aligned}
N_\varphi &\ge 2R_0b_0 \\
N_r &\ge 2R_0b_0/\pi\,,
\end{aligned}$$

for sampling the circular Radon transform $\mathbf{M}_R f$ of an essentially b_0-bandlimited function supported in $D(R_0)$. For the special case that $R_0 = R$, this reduces to the sampling scheme (3)-(5) with the sampling conditions (6), (7) presented in the introduction.

D. Numerical results

For all simulations presented in this subsection we consider the circular Radon transform $\mathbf{M}_R f$ for $R = 1$. Numerical approximations of $\mathbf{M}_R f$ are computed by applying the composition trapezoidal rule in the angular variable. Numerical reconstructions of f from samples $\mathbf{M}_R f(\varphi_k, r_\ell)$ are computed using the numerical implementation of the inversion formula [11, Eq. (1.5)] as described in [11, Section 4].

We first illustrate the support of $\mathbf{FM}_R f$. For that purpose we consider a function $f\colon \mathbb{R}^2 \to \mathbb{R}$ with essential bandwidth $b_0 = 170$ and support in $D(R_0)$ with $R_0 = 0.7$. The phantom f and a logarithmic plot of $\mathbf{FM}_R f$ are shown in Figure 5. We observe that $\mathbf{FM}_R f$ is exponentially decreasing outside a rectangle $Q(b_0R_0/c, b_0)$ where c is close to one. In fact, it seems that $\mathbf{FM}_R f$ is actually exponentially decreasing outside $S(c,b_0,R_0) \subseteq Q(b_0R_0/c,b_0)$. However, our current analysis does not support such a stronger result.

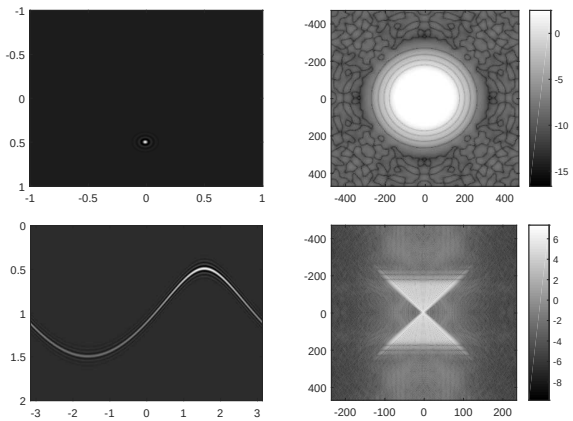

Fig. 5. BANDLIMITED FUNCTION. Top Left: Essentially b_0-bandlimited function $f \in C_c^\infty(D(R_0))$. Top Right: Logarithm $\log|\mathbf{F}f|$ of magnitude of Fourier spectrum $\mathbf{F}f$. Bottom Left: Circular Radon transform $\mathbf{M}_R f$. Bottom Right: Logarithm $\log|\mathbf{FM}_R f|$ of magnitude of Fourier spectrum $\mathbf{FM}_R f$.

Next we compare numerical reconstructions using either sufficient or insufficient sampling. We only present results for

angular undersampling, since usually in practical applications the number of angular samples is the limiting factor. For that purpose we first use the same essentially b_0-bandlimited phantom shown in Figure 5. The reconstruction results are shown in Figure 6. The top row shows the results using correct sampling, whereas the bottom row shows reconstruction results using an angular undersampling factor of 0.8 and 0.6, respectively. In the latter reconstructions one clearly notices ring-shaped artifacts that arise from angular undersampling.

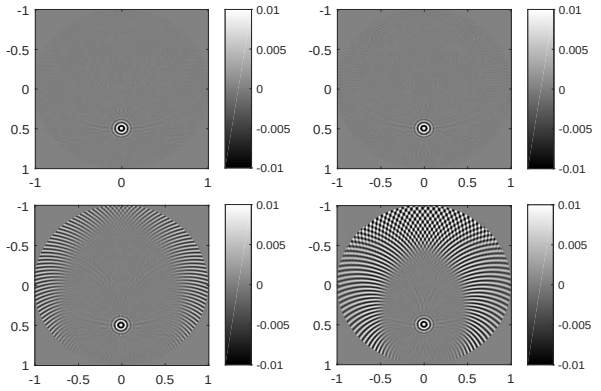

Fig. 6. RECONSTRUCTION ERROR $f - f_c$ FOR RECOVERING THE PHANTOM OF FIGURE 5 USING DIFFERENT NUMBERS OF ANGULAR SAMPLES. Top Left: Oversampling by factor $c = 1.2$. Top Right: Full sampling ($N_\varphi = 2b_0R_0$; oversampling factor $c = 1$). Bottom Left: undersampling by factor $c = 0.8$ Bottom Right: undersampling by factor $c = 0.6$.

Finally, we present reconstruction results for a non-bandlimited phantom. The top row in Figure 7 shows reconstructions using different angular sampling rates for data with and without noise. The phantom is discretized using $N_r = 301$ spatial samples, which is equal to the number of radial samples used for discretizing $\mathbf{M}_R f$. One notices that for exact data using full angular sampling one obtains almost perfect reconstruction (Figure 1, top left). Also after adding noise (Figure 1, top center) and using angular undersampling (Figure 1, top right) one obtains results quite close to the original phantom. However, in the reconstruction from under-sampled data one clearly notes circularly shaped undersampling artifacts. The bottom row in Figure 1 shows the Fourier spectrum of the phantom, the data and the reconstruction from under-sampled data.

V. DISCUSSION

In this paper we analyzed sampling of the circular Radon transform $\mathbf{M}_R f$ in circular geometry. Under the assumptions that f is supported in $D(R)$ and that it is essentially b_0-bandlimited we derived the sampling conditions $N_\varphi \geq 2Rb_0$ for the number of angular samples in $[0, 2\pi)$ and $N_r \geq 2Rb_0/\pi$ for the number of radial samples in $[0, 2R]$. These are the same conditions as for sampling the classical two dimensional Radon transform of an essentially b_0-bandlimited supported in $D(R)$.

The classical Radon transform satisfies the symmetry property $\mathbf{R}(-\theta, -s) = \mathbf{R}(\theta, s)$. Therefore only half of the samples of $\mathbf{R}f$ have actually to be measured in practice [25]. Consequently, an essentially b_0-bandlimited function $f \in C_c(D(R))$

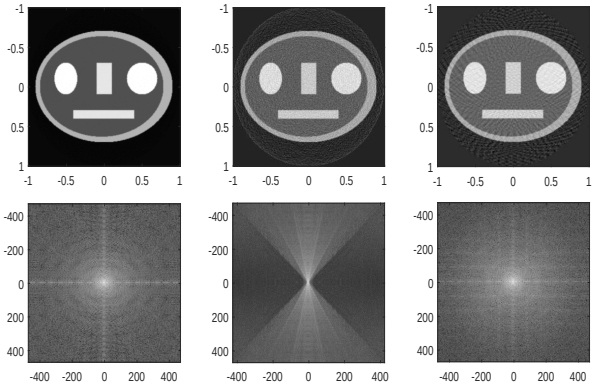

Fig. 7. RECONSTRUCTIONS USING A NON-BANDLIMITED PHANTOM. Top Left: Reconstruction from simulated data using $N_r = 300$ and $N_\phi = 848$ (full angular sampling). Top Center: Reconstruction from fill angular sampling where 5% noise has been added to the circular radon transform. Top Right: Reconstruction from simulated data using $N_r = 300$ and $N_\phi = 85$ (angular undersampling). Bottom Left: Fourier spectrum $\log|\mathbf{F}f|$ of the original phantom. Bottom Left: Fourier spectrum $\log|\mathbf{F}\mathbf{M}_R f|$ of the data. Bottom Left: Fourier spectrum $\log|\mathbf{F}f_{\text{rec}}|$ of the reconstructed phantom form angular under-sampled data.

can be stably recovered from $2R^2b_0^2/\pi$ Radon samples on the standard grid. Due to the absence of an analogous symmetry property of the circular Radon transform, we require $4R^2b_0^2/\pi$ samples of the circular Radon transform for recovering the same function, which is twice the number of Radon samples. It would be interesting to find out if and how the number of samples for circular Radon transform can also be reduced by exploiting certain range conditions [35]–[37]. Range conditions may also be used to reduce the coverage of the measurement aperture with respect to θ, leading to a so called limited angle problem [37]. To reduce the number of required angular sampling points and angular coverage one may additionally exploit multiple reflections (see [38]–[41]).

The number of Radon samples can further be reduced to $R^2b_0^2/\pi$ when using the interlaced lattice instead of the standard lattice. In order to obtain such a result for the circular Radon transform we would require showing that $\mathbf{F}\mathbf{M}_R f$ is essentially supported in $S(c, b_0, R_0)$. Whereas our current analysis does not yields such a result, numerical simulations (see Figure 5) indicate that this might by the case.

Finally, we note that in practical applications, such as in photoacoustic tomography, the original function f itself will usually not be essentially bandlimited for some reasonable bandwidth $b_0 > 0$. However, due to attenuation, the finite bandwidth of the detection system and other practical issues (see [1], [4], [42], [43]), the measured data $g \simeq \mathbf{M}_R f(\varphi, \cdot)$ in photoacoustic tomography are actually essentially bandlimited with some maximal frequency ω_0. Our sampling conditions show that in such a situation maximal $N_\varphi = 2R\omega_0$ angular samples have to be collected.

APPENDIX A
PROOF OF LEMMA III.1

A. Auxiliary result

Let $\mathbf{R}f(\theta, s) := \int_{\mathbb{R}} f(s\theta + t\theta^\perp)\mathrm{d}t$, for $(\theta, s) \in \mathbb{S}^1 \times \mathbb{R}$, denote the classical Radon transform of $f \in C_c^\infty(D(R))$.

Further, for a smooth function $h_0\colon \mathbb{R} \to \mathbb{R}$ denote by $\mathbf{U}_s h_0\colon \mathbb{R}\times\mathbb{R}\to\mathbb{R}$ the solution of the one-dimensional wave equation $(\partial_t^2 - \partial_s^2)h(x,t) = 0$ for $(s,t)\in\mathbb{R}^2$ with the initial conditions $h(s,0) = h_0(s)$ and $(\partial_t h)(s,0) = 0$. Finally, for $g \in C_c^\infty(\mathbb{S}^1\times\mathbb{R})$ we define the Riesz potential $\mathbf{I}_t g$ by $\mathbf{F}_t(\mathbf{I}_t g)(\theta,\omega) \coloneqq |\omega|(\mathbf{F}_t g)(\theta,\omega)$ for $(\theta,\omega)\in\mathbb{S}^1\times\mathbb{R}$.

Lemma A.1. *For all $f \in C_c^\infty(D(R))$ and $(z,\omega)\in\mathbb{R}^2\times\mathbb{R}$,*

$$(\mathbf{F}_t\mathbf{U}f)(z,\omega) = \frac{|\omega|}{2\sqrt{2\pi}}\int_{\mathbb{S}^1}(\mathbf{F}f)(\omega\theta)e^{i\omega\langle\theta,z\rangle}\mathrm{d}\theta\,. \tag{28}$$

Proof: We start by deriving an auxiliary representation of $\mathbf{U}f$ in terms of $\mathbf{R}f$. The commutation relation $\mathbf{R}\Delta = \partial_s^2\mathbf{R}$ implies that $\mathbf{R}\mathbf{U}f = \mathbf{U}_s\mathbf{R}f$. We further have:

1) $\mathbf{U}f = \mathbf{R}^{-1}\mathbf{R}\mathbf{U}f = \mathbf{R}^{-1}\mathbf{U}_s\mathbf{R}f$;
2) $\mathbf{R}^{-1}g(z) = \frac{1}{4\pi}\int_{\mathbb{S}^1}(\mathbf{I}_t g)(\theta,\langle\theta,z\rangle)\mathrm{d}\theta$;
3) $\mathbf{U}_s(\mathbf{R}f)(s,t) = \frac{1}{2}((\mathbf{R}f)(s+t) + (\mathbf{R}f)(s-t))$.

Combining 1)-3) yields

$$\begin{aligned}(\mathbf{U}f)(z,t) &= \frac{1}{8\pi}\int_{\mathbb{S}^1}\big((\mathbf{I}_t\mathbf{R}f)(\theta,\langle\theta,z\rangle+t)\\ &\qquad + (\mathbf{I}_t\mathbf{R}f)(\theta,\langle\theta,z\rangle - t)\big)\mathrm{d}\theta\\ &= \frac{1}{8\pi}\int_{\mathbb{S}^1}\big((\mathbf{I}_t\mathbf{R}f)(\theta,\langle\theta,z\rangle+t)\\ &\qquad + (\mathbf{I}_t\mathbf{R}f)(-\theta,-\langle\theta,z\rangle - t)\big)\mathrm{d}\theta\\ &= \frac{1}{4\pi}\int_{\mathbb{S}^1}(\mathbf{I}_t\mathbf{R}f)(\theta,\langle\theta,z\rangle+t)\mathrm{d}\theta\,.\end{aligned} \tag{29}$$

Here the second identity follows by substituting θ with $-\theta$ when integrating the second summand, and the last identity follows from $\mathbf{R}f(-\theta,-s) = \mathbf{R}f(\theta,s)$.

Application of $\mathbf{F}_t$ to (29) yields

$$\begin{aligned}(\mathbf{F}_t\mathbf{U}f)(z,\omega) &= \frac{1}{4\pi}\int_{\mathbb{S}^1}\mathbf{F}[t\mapsto(\mathbf{I}_t\mathbf{R}f)(\theta,\langle\theta,z\rangle+t)](\omega)\mathrm{d}\theta\\ &= \frac{1}{4\pi}\int_{\mathbb{S}^1}(\mathbf{F}_t\mathbf{I}_t\mathbf{R}f)(\theta,\omega)e^{i\omega\langle\theta,z\rangle}\mathrm{d}\theta\\ &= \frac{1}{4\pi}\int_{\mathbb{S}^1}|\omega|(\mathbf{F}_t\mathbf{R}f)(\theta,\omega)e^{i\omega\langle\theta,z\rangle}\mathrm{d}\theta\\ &= \frac{|\omega|}{2\sqrt{2\pi}}\int_{\mathbb{S}^1}(\mathbf{F}f)(\omega\theta)e^{i\omega\langle\theta,z\rangle}\mathrm{d}\theta\,,\end{aligned}$$

which is the desired identity (28). Here, for the last equality we have made use of the Fourier slice identity [25]. ∎

B. Proof of Equation (14)

Lemma A.1 yields

$$\begin{aligned}&(\mathbf{F}\mathbf{U}_R f)(k,\omega)\\ &= \frac{1}{\sqrt{2\pi}}\int_0^{2\pi}(\mathbf{F}_t\mathbf{U}_R f)(\varphi,s)e^{-ik\varphi}\mathrm{d}\varphi\\ &= \frac{|\omega|}{4\pi}\int_0^{2\pi}\int_{\mathbb{S}^1}(\mathbf{F}f)(\omega\theta)e^{i\omega\langle\theta,z(\varphi)\rangle}e^{-ik\varphi}\mathrm{d}\theta\mathrm{d}\varphi\,.\end{aligned}$$

Next recall the integral representation of the k-th order Bessel function, $J_k(u) = i^{-k}/(2\pi)\int_0^{2\pi}e^{iu\cos(\varphi)-ik\varphi}\mathrm{d}\varphi$. Writing $\theta(\alpha) = (\cos(\alpha),\sin(\alpha))$, interchanging the order of integration, and applying the integral representation yields

$$\begin{aligned}&(\mathbf{F}\mathbf{U}_R f)(k,\omega)\\ &= \frac{|\omega|}{4\pi}\int_0^{2\pi}\int_0^{2\pi}(\mathbf{F}f)(\omega\theta(\alpha))e^{i\omega R\cos(\alpha-\varphi)-ik\varphi}\mathrm{d}\alpha\mathrm{d}\varphi\\ &= \frac{|\omega|}{4\pi}\int_0^{2\pi}(\mathbf{F}f)(\omega\theta(\alpha))\int_0^{2\pi}e^{i\omega R\cos(\alpha-\varphi)-ik\varphi}\mathrm{d}\varphi\mathrm{d}\alpha\\ &= \frac{|\omega|}{4\pi}\int_0^{2\pi}(\mathbf{F}f)(\omega\theta(\alpha))e^{-ik\alpha}\int_0^{2\pi}e^{i\omega R\cos(\varphi)-ik\varphi}\mathrm{d}\varphi\mathrm{d}\alpha\\ &= \frac{i^k}{2}|\omega|J_k(\omega R)\int_0^{2\pi}(\mathbf{F}f)(\omega\theta(\alpha))e^{-ik\alpha}\mathrm{d}\alpha\,.\end{aligned}$$

C. Proof of Equation (15)

Using (14) and the definition of the Fourier transform on $\mathbb{R}^2$ and interchanging the order of integration yields

$$\begin{aligned}&(\mathbf{F}\mathbf{U}_R f)(k,\omega)\\ &= \frac{i^k}{4\pi}|\omega|J_k(\omega R)\int_0^{2\pi}\int_{\mathbb{R}^2}f(x)e^{-i\omega\langle\theta(\alpha),x\rangle}\mathrm{d}x e^{-ik\alpha}\mathrm{d}\alpha\\ &= \frac{i^k}{4\pi}|\omega|J_k(\omega R)\int_{\mathbb{R}^2}f(x)\int_0^{2\pi}e^{-i\omega\|x\|\cos(\alpha-\beta)-ik\alpha}\mathrm{d}\alpha\mathrm{d}x\\ &= \frac{i^k}{4\pi}|\omega|J_k(\omega R)\int_{\mathbb{R}^2}f(x)e^{-ik\beta}\int_0^{2\pi}e^{-i\omega\|x\|\cos(\alpha)-ik\alpha}\mathrm{d}\alpha\mathrm{d}x\\ &= \frac{(-1)^k}{2}|\omega|J_k(\omega R)\int_{\mathbb{R}^2}f(x)e^{-ik\beta}J_k(-\omega\|x\|)\mathrm{d}x\,.\end{aligned}$$

Here, $\beta = \arg(x)$ denotes the argument of x. Finally, using $J_k(-\omega\|x\|) = (-1)^k J_k(\omega\|x\|)$ yields (15).

REFERENCES

[1] P. Beard, "Biomedical photoacoustic imaging," *Interface focus*, vol. 1, no. 4, pp. 602–631, 2011.

[2] G. Paltauf, R. Nuster, M. Haltmeier, and P. Burgholzer, "Photoacoustic tomography using a Mach-Zehnder interferometer as an acoustic line detector," *App. Opt.*, vol. 46, no. 16, pp. 3352–3358, 2007.

[3] L. V. Wang, "Multiscale photoacoustic microscopy and computed tomography," *Nature Phot.*, vol. 3, no. 9, pp. 503–509, 2009.

[4] M. Xu and L. V. Wang, "Photoacoustic imaging in biomedicine," *Rev. Sci. Instruments*, vol. 77, no. 4, p. 041101 (22pp), 2006.

[5] S. J. Norton, "Reconstruction of a two-dimensional reflecting medium over a circular domain: Exact solution," *J. Acoust. Soc. Amer.*, vol. 67, no. 4, pp. 1266–1273, 1980.

[6] S. J. Norton and M. Linzer, "Ultrasonic reflectivity imaging in three dimensions: Exact inverse scattering solutions for plane, cylindrical and spherical apertures," *IEEE Trans. Biomed. Eng.*, vol. 28, no. 2, pp. 202–220, 1981.

[7] A. C. Kak and M. Slaney, *Principles of Computerized Tomographic Imaging*, ser. Classics in Applied Mathematics. Philadelphia, PA: Society for Industrial and Applied Mathematics (SIAM), 2001, vol. 33.

[8] P. Burgholzer, C. Hofer, G. Paltauf, M. Haltmeier, and O. Scherzer, "Thermoacoustic tomography with integrating area and line detectors," *IEEE Trans. Ultrason., Ferroeletr., Freq. Control*, vol. 52, no. 9, pp. 1577–1583, September 2005.

[9] P. Burgholzer, J. Bauer-Marschallinger, H. Grün, M. Haltmeier, and G. Paltauf, "Temporal back-projection algorithms for photoacoustic tomography with integrating line detectors," *Inverse Probl.*, vol. 23, no. 6, pp. S65–S80, 2007.

[10] G. Paltauf, R. Nuster, M. Haltmeier, and P. Burgholzer, "Experimental evaluation of reconstruction algorithms for limited view photoacoustic tomography with line detectors," *Inverse Probl.*, vol. 23, no. 6, pp. S81–S94, 2007.

[11] D. Finch, M. Haltmeier, and Rakesh, "Inversion of spherical means and the wave equation in even dimensions," *SIAM J. Appl. Math.*, vol. 68, no. 2, pp. 392–412, 2007.

[12] M. Haltmeier, "Inversion of circular means and the wave equation on convex planar domains," *Comput. Math. Appl.*, vol. 65, no. 7, pp. 1025–1036, 2013.

[13] L. A. Kunyansky, "Explicit inversion formulae for the spherical mean Radon transform," *Inverse Probl.*, vol. 23, no. 1, pp. 373–383, 2007.

[14] ——, "Fast reconstruction algorithms for the thermoacoustic tomography in certain domains with cylindrical or spherical symmetries," *Inverse Probl. Imaging*, vol. 6, no. 1, pp. 111–131, 2012.
[15] V. P. Palamodov, "A uniform reconstruction formula in integral geometry," *Inverse Probl.*, vol. 28, no. 6, p. 065014, 2012.
[16] Y. Salman, "An inversion formula for the spherical mean transform with data on an ellipsoid in two and three dimensions," *J. Math. Anal. Appl.*, vol. 420, pp. 612–620, 2014.
[17] M. Xu and L. V. Wang, "Universal back-projection algorithm for photoacoustic computed tomography," *Phys. Rev. E*, vol. 71, no. 1, p. 016706, 2005.
[18] G. Beylkin, "Discrete Radon transform," *IEEE Trans. Acoust., Speech, Signal Processing*, vol. 35, no. 2, pp. 162–172, 1987.
[19] A. M. Cormack, "Sampling the radon transform with beams of finite width," *Phys. Med. Biol.*, vol. 23, no. 6, pp. 1141–1148, 1978.
[20] L. Desbat, "Efficient sampling on coarse grids in tomography," *Inverse Problems*, vol. 9, no. 2, pp. 251–269, 1993.
[21] A. Faridani, "Reconstructing from efficiently sampled data in parallel-beam computed tomography," in *Inverse problems and imaging (Glasgow, 1988)*, ser. Pitman Res. Notes Math. Ser. Longman Sci. Tech., Harlow, 1991, vol. 245, pp. 68–102.
[22] ——, "Sampling in parallel-beam tomography," in *Inverse problems, tomography, and image processing (Newark, DE, 1997)*. Plenum, New York, 1998, pp. 33–53.
[23] ——, "Fan-beam tomography and sampling theory," in *The Radon transform, inverse problems, and tomography*, ser. Proc. Sympos. Appl. Math. Amer. Math. Soc., Providence, RI, 2006, vol. 63, pp. 43–66.
[24] F. Natterer, "Sampling in fan beam tomography," *SIAM J. Appl. Math.*, vol. 53, no. 2, pp. 358–380, 1993.
[25] ——, *The Mathematics of Computerized Tomography*, ser. Classics in Applied Mathematics. Philadelphia: SIAM, 2001, vol. 32.
[26] P. Rattey and A. G. Lindgren, "Sampling the 2-D radon transform," *IEEE Trans. Acoust., Speech, Signal Processing*, vol. 29, no. 5, pp. 994–1002, 1981.
[27] G. Beylkin, "The inversion problem and applications of the generalized Radon transform," *Comm. Pure Appl. Math.*, vol. 37, no. 5, pp. 579–599, 1984.
[28] A. J. Jerri, "The shannon sampling theorem—its various extensions and applications: A tutorial review," *Proc. IEEE*, vol. 65, no. 11, pp. 1565–1596, 1977.
[29] P. P. Petersen and D. Middleton, "Sampling and reconstruction of wave-numberlimited functions in n-dimensional euclidean space," *Inform. Control*, vol. 5, pp. 279–323, 1962.
[30] C. E. Shannon, "Communication in the presence of noise," *Proceedings of the IRE*, vol. 37, no. 1, pp. 10–21, Jan 1949.
[31] M. Unser, "Sampling—50 Years after Shannon," *Proc. IEEE*, vol. 88, no. 4, pp. 569–587, 2000.
[32] L. C. Evans, *Partial Differential Equations*, ser. Graduate Studies in Mathematics. Providence, RI: American Mathematical Society, 1998, vol. 19.
[33] Y. Xu, M. Xu, and L. V. Wang, "Exact frequency-domain reconstruction for thermoacoustic tomography–II: Cylindrical geometry," *IEEE Trans. Med. Imag.*, vol. 21, pp. 829–833, 2002.
[34] A. Erdélyi, W. Magnus, F. Oberhettinger, and F. G. Tricomi, *Tables of integral transforms. Vol. I.* McGraw-Hill Book Company, Inc., New York-Toronto-London, 1954, based, in part, on notes left by Harry Bateman.
[35] M. Agranovsky, D. Finch, and P. Kuchment, "Range conditions for a spherical mean transform," *Inverse Probl. Imaging*, vol. 3, no. 3, pp. 373–383, 2009.
[36] G. Ambartsoumian and P. Kuchment, "A range description for the planar circular Radon transform," *SIAM J. Math. Anal.*, vol. 38, no. 2, pp. 681–692, 2006.
[37] S. Patch, "Thermoacoustic tomography; consistency conditions and the partial scan problem," *Phys. Med. Biol.*, vol. 49, pp. 2305–2315, 2004.
[38] R. Ellwood, E. Zhang, P. Beard, and B. Cox, "Photoacoustic imaging using acoustic reflectors to enhance planar arrays," *J. Biomed. Opt.*, vol. 19, no. 12, p. 126012, 2014.
[39] L. Kunyansky, B. Holman, and B. T. Cox, "Photoacoustic tomography in a rectangular reflecting cavity," *Inverse Probl.*, vol. 29, no. 12, pp. 125 010, 20, 2013.
[40] C. J. Nolan, M. Cheney, T. Dowling, and R. Gaburro, "Enhanced angular resolution from multiply scattered waves," *Inverse Probl.*, vol. 22, no. 5, pp. 1817–1834, 2006.
[41] D. Wu, X. Wang, C. Tao, and X. J. Liu, "Limited-view photoacoustic tomography utilizing backscatterers as virtual transducers," *Appl. Phys. Lett.*, vol. 99, no. 24, p. 244102, 2011.
[42] M. Haltmeier and G. Zangerl, "Spatial resolution in photoacoustic tomography: Effects of detector size and detector bandwidth," *Inverse Probl.*, vol. 26, no. 12, p. 125002, 2010.
[43] M. Xu and L. V. Wang, "Analytic explanation of spatial resolution related to bandwidth and detector aperture size in thermoacoustic or photoacoustic reconstruction," *Phys. Rev. E*, vol. 67, no. 5, pp. 0 566 051–05 660 515 (electronic), 2003.